Quantized superfluid vortex dynamics on cylindrical surfaces and planar annuli

Nils-Eric Guenther,[1,*] Pietro Massignan,[2,1,†] and Alexander L. Fetter[3,‡]

[1]*ICFO–Institut de Ciències Fotòniques, The Barcelona Institute of Science and Technology, E-08860 Castelldefels (Barcelona), Spain*

[2]*Departament de Física, Universitat Politècnica de Catalunya, Campus Nord B4-B5, E-08034 Barcelona, Spain*

[3]*Departments of Physics and Applied Physics, Stanford University, Stanford, California 94305-4045, USA*

(Received 1 September 2017; published 6 December 2017)

Superfluid vortex dynamics on an infinite cylinder differs significantly from that on a plane. The requirement that a condensate wave function be single valued upon once encircling the cylinder means that such a single vortex cannot remain stationary. Instead, it acquires one of a series of quantized translational velocities around the circumference, the simplest being $\pm\hbar/(2MR)$, with M the mass of the superfluid particles and R the radius of the cylinder. A generalization to a finite cylinder automatically includes these quantum-mechanical effects through the pairing of the single vortex and its image in either the top or bottom end of the surface. The dynamics of a single vortex on this surface provides a hydrodynamic analog of Laughlin pumping. The interaction energy for two vortices on an infinite cylinder is proportional to the classical stream function $\chi(\boldsymbol{r}_{12})$, and it crosses over from logarithmic to linear when the intervortex separation $\boldsymbol{r}_{12}$ becomes larger than the cylinder radius. An appendix summarizes the connection to an earlier study of Ho and Huang for one or more vortices on an infinite cylinder. A second appendix reviews the topologically equivalent planar annulus, where such quantized vortex motion has no offset, but Laughlin pumping may be more accessible to experimental observation.

DOI: 10.1103/PhysRevA.96.063608

I. INTRODUCTION

The dynamics of point vortices in an incompressible nonviscous fluid has been of great interest since the late 19th century [1]. For example, given an initial vortex configuration, the subsequent motion obeys first-order equations of motion, which differs greatly from the usual second-order Newtonian equations describing point masses. In addition, the x and y coordinates of each vortex serve as canonical variables, analogous to x and p for a Newtonian point particle.

This description has found wide application to superfluid ^{4}He which acts like an incompressible fluid for vortex motion much slower than the speed of sound ∼240 m/s [2]. Such superfluid systems involve a complex macroscopic condensate wave function $\Psi = |\Psi|e^{i\Phi}$, whose phase Φ determines the superfluid velocity $\boldsymbol{v} = \hbar\nabla\Phi/M$, where M is the atomic mass. In this way, the quantum-mechanical phase Φ becomes the velocity potential. The creation of dilute ultracold superfluid atomic Bose-Einstein condensates (BECs) in 1995 has subsequently stimulated many new applications of the same formalism [3–5].

Classical nonviscous irrotational and incompressible hydrodynamics describes well the dynamics of vortices in superfluid ^{4}He, with the additional condition of quantized circulation [2]. Although dilute ultracold superfluid BECs are compressible, local changes in the density become small in the Thomas-Fermi (TF) limit, which typically describes many important experiments [6]. In this limit, the condition of current conservation for steady flow $\nabla\cdot(n\boldsymbol{v}) = 0$ reduces to the condition of incompressibility $\nabla\cdot\boldsymbol{v} = 0$. For such incompressible flow, the stream function χ provides an important alternative description of the superfluid flow. Specifically, for two-dimensional flow in the xy plane, the velocity becomes

$$\boldsymbol{v} = (\hbar/M)\,\hat{\boldsymbol{n}}\times\nabla\chi, \tag{1}$$

where $\hat{\boldsymbol{n}} = \hat{\boldsymbol{x}}\times\hat{\boldsymbol{y}}$ is the unit vector normal to the two-dimensional plane, following the right-hand rule.

For such irrotational incompressible flow in two dimensions (x,y), the complex variable $z = x + iy$ provides a natural framework for vortex dynamics. It is helpful to introduce a complex potential $F(z) = \chi(\boldsymbol{r}) + i\Phi(\boldsymbol{r})$, with $\boldsymbol{r} = (x,y)$. For any such analytic function, the Cauchy-Riemann conditions yield the components of velocity:

$$v_x = \frac{\hbar}{M}\frac{\partial\Phi}{\partial x} = -\frac{\hbar}{M}\frac{\partial\chi}{\partial y} \quad\text{and}\quad v_y = \frac{\hbar}{M}\frac{\partial\Phi}{\partial y} = \frac{\hbar}{M}\frac{\partial\chi}{\partial x}. \tag{2}$$

These conditions give the compact representation of the hydrodynamic flow velocity components,

$$v_y + i\,v_x = (\hbar/M)\,F'(z), \tag{3}$$

in terms of the first derivative $F'(z)$ of the complex potential.

Note that the representation of $\boldsymbol{v}$ in terms of the velocity potential Φ ensures that the flow is irrotational (namely $\nabla\times\boldsymbol{v} = \boldsymbol{0}$), apart from singularities associated with the vortex cores. This applies to all superfluids in both two and three dimensions. In contrast, the representation in terms of the stream function ensures that the flow is incompressible with $\nabla\cdot\boldsymbol{v} = 0$, for it can be rewritten as $\boldsymbol{v} = -(\hbar/M)\nabla\times(\hat{\boldsymbol{n}}\chi)$. This condition does not apply generally to all superfluids, but it can be very useful in many specific cases.

For flow in a plane, the stream function $\chi(\boldsymbol{r})$ has the special advantage that χ takes a constant value along a streamline of the hydrodynamic flow. In addition, as shown below, the interaction energy between two vortices at $\boldsymbol{r}_1$ and $\boldsymbol{r}_2$ is directly proportional to $\chi(\boldsymbol{r}_{12})$, where $\boldsymbol{r}_{12} = \boldsymbol{r}_1 - \boldsymbol{r}_2$ is the intervortex separation, as discussed in [7].

*nils.guenther@icfo.eu

†pietro.massignan@upc.edu

‡fetter@stanford.edu

All these results are familiar in the case of point vortices in a plane. For example, the complex potential for a positive unit vortex at the origin is $F(Z) = \ln Z = \ln r + i\phi$, where $r = \sqrt{X^2 + Y^2}$ and $\tan\phi = Y/X$. Hence $F'(Z) = 1/Z$. It is not difficult to verify that $\boldsymbol{v} = (\hbar/Mr)\hat{\boldsymbol{\phi}}$ and that the vorticity $\boldsymbol{\zeta} = \boldsymbol{\nabla} \times \boldsymbol{v}$ is singular, with $\boldsymbol{\zeta} = (2\pi\hbar/M)\,\hat{\boldsymbol{n}}\,\delta^{(2)}(\boldsymbol{r})$. It follows from familiar vector identities that the stream function for a point vortex at the origin obeys an inhomogeneous equation with the vorticity as its source:

$$\nabla^2\chi(\boldsymbol{r}) = 2\pi\delta^{(2)}(\boldsymbol{r}), \tag{4}$$

and is thus effectively a two-dimensional Coulomb Green's function. In general, the stream function also satisfies various boundary conditions. Typically, boundaries break translational invariance, and the stream function depends symmetrically on the two variables: $\chi(\boldsymbol{r},\boldsymbol{r}_j) = \chi(\boldsymbol{r}_j,\boldsymbol{r})$.

More recently, the behavior of singularities in various order parameters on curved surfaces has attracted great interest. The simplest such case is a superfluid vortex with a single complex order parameter, although liquid crystals present many more intricate examples [8,9].

Here we focus on the dynamics of point vortices in a thin superfluid film on a cylindrical surface of radius R. We start with an infinite cylinder in Sec. II and show that the identification of the velocity potential as the quantum-mechanical phase Φ requires a single vortex to move uniformly around the cylinder with (in the simplest case) one of two specific quantized values.

In Sec. III we study the dynamics of two vortices on a cylinder, which is unexpectedly rich. Vortices with opposite signs move uniformly perpendicular to the relative vector $\boldsymbol{r}_{12}$, in the direction of the flow between them. This behavior is closely related to the quantized vortex velocity found in Sec. II. In contrast, two such vortices with the same sign maintain their centroid $\boldsymbol{R}_{12} = \frac{1}{2}(\boldsymbol{r}_1 + \boldsymbol{r}_2)$, displaying both bound orbits and unbounded orbits, in close analogy to the motion of a simple pendulum.

In Sec. IV, we evaluate the interaction energy E_{12} of two vortices, relating it to the relevant stream function $\chi(\boldsymbol{r}_{12})$. This result allows us to re-express the dynamics of two or more vortices in terms of forces, including the Magnus force [7].

Section V considers a vortex on a finite cylinder of length L, where the method of images provides an exact solution in terms of the first Jacobi ϑ function [10,11]. The resulting dynamics under the action of additional external rotation constitutes a direct hydrodynamic analog of the Laughlin pumping.

Previously, Ho and Huang [12] studied spinor condensates on a cylindrical surface and found some of the results that we present here. Appendix A compares the two approaches.

Appendix B reviews the annular geometry in a plane, considered in Ref. [11]. The geometry of a planar annulus is topologically equivalent to that of a finite cylinder, so that the vortex dynamics on these two surfaces have some close resemblances.

II. POINT VORTEX ON AN INFINITE CYLINDER

On the surface of a cylinder of radius R, let $-\pi R \leqslant x \leqslant \pi R$ represent the coordinate around the circumference and $-\infty \leqslant y \leqslant \infty$ the unbounded coordinate along the cylinder's axis. The unit vector $\hat{\boldsymbol{n}}$ is then the outward normal to the surface of the cylinder. For a thin superfluid film, the problem is apparently equivalent to the infinite plane with periodic repetitions of a strip of width $2\pi R$ along $\hat{\boldsymbol{x}}$. As seen below, however, this classical picture violates the quantum-mechanical requirement of a single-valued condensate wave function once encircling the cylinder. We find that a single vortex on an infinite cylinder must move around the cylinder with a set of quantized velocities.

Throughout this section we consider a single point vortex at the origin of the cylindrical surface ($x = 0, y = 0$). Note that x/R is just the azimuthal angle ϕ in cylindrical polar coordinates. With the usual complex notation $z = x + iy$ and $f(z)$ a function of this complex variable, the complex potential $F(z) = \ln f(z)$ corresponds to a positive vortex at each zero of $f(z)$. In particular, Sec. 156 of [1] notes that the choice,

$$F(z) = \ln\left[\sin\left(\frac{z}{2R}\right)\right], \tag{5}$$

represents a one-dimensional periodic array of positive vortices at positions $z_n = 2\pi nR$, with $n \in \mathbb{Z}$.

At first sight, this complex potential should also represent a single superfluid vortex at the origin of an infinite cylinder. Note, however, that $\sin(z/2R)$ changes sign for $z \to z + 2\pi R$. Consequently, the present velocity potential $\Phi(\boldsymbol{r}) = \mathrm{Im}F(z)$ is not acceptable as the phase of a single-valued quantum-mechanical condensate wave function, because $e^{i\Phi(\boldsymbol{r})}$ remains unchanged only for $x \to x + 4\pi R$.

A. Velocity potential for one vortex on a cylinder: classical hydrodynamics vs quantized superfluidity

Here, we explore the source of this discrepancy by evaluating in detail the velocity potential,

$$\Phi(\boldsymbol{r}) = \mathrm{Im}\ln\left[\sin\left(\frac{z}{2R}\right)\right] = \arctan\left[\frac{\tanh(y/2R)}{\tan(x/2R)}\right]. \tag{6}$$

As expected, this reduces to $\arctan(y/x)$ for $r \ll R$.

In the quantum interpretation, the velocity potential Φ is also the phase of the condensate wave function, which leads to the following inconsistency: Note that Φ increases by $\mp\mathrm{sgn}(y)\pi$ when $x \to x + 2\pi R$, where $\mathrm{sgn}(y) = |y|/y$. Hence the condensate wave function would be antiperiodic once going around the cylinder. As seen below, the actual fluid velocity itself is indeed continuous and periodic, so that this complex potential is acceptable as a classical solution but not as a quantum mechanical one if the vortex itself remains at rest.

Consider the lines of constant phase. For a single vortex on a plane, these lines extend radially from the center of the vortex, rather like electric field lines from a two-dimensional point charge. On a cylinder, the periodicity means that half the phase lines go upward and half go downward (see Fig. 1 top row). The net change in phase on going once around the circumference of the cylinder is $\mp\pi$, depending on the sign of y.

An illuminating way to think about this question focuses on a vorticity flux of 2π associated with a singly quantized vortex (measured in units of $\hbar/M$). For a positive stationary vortex with charge $q = 1$ at the origin of the surface, the flux comes from inside the cylinder and emerges radially outward along $\hat{\boldsymbol{n}}$ through the center of the vortex. In the present case of a vortex at rest, the flux comes symmetrically with π flowing downward

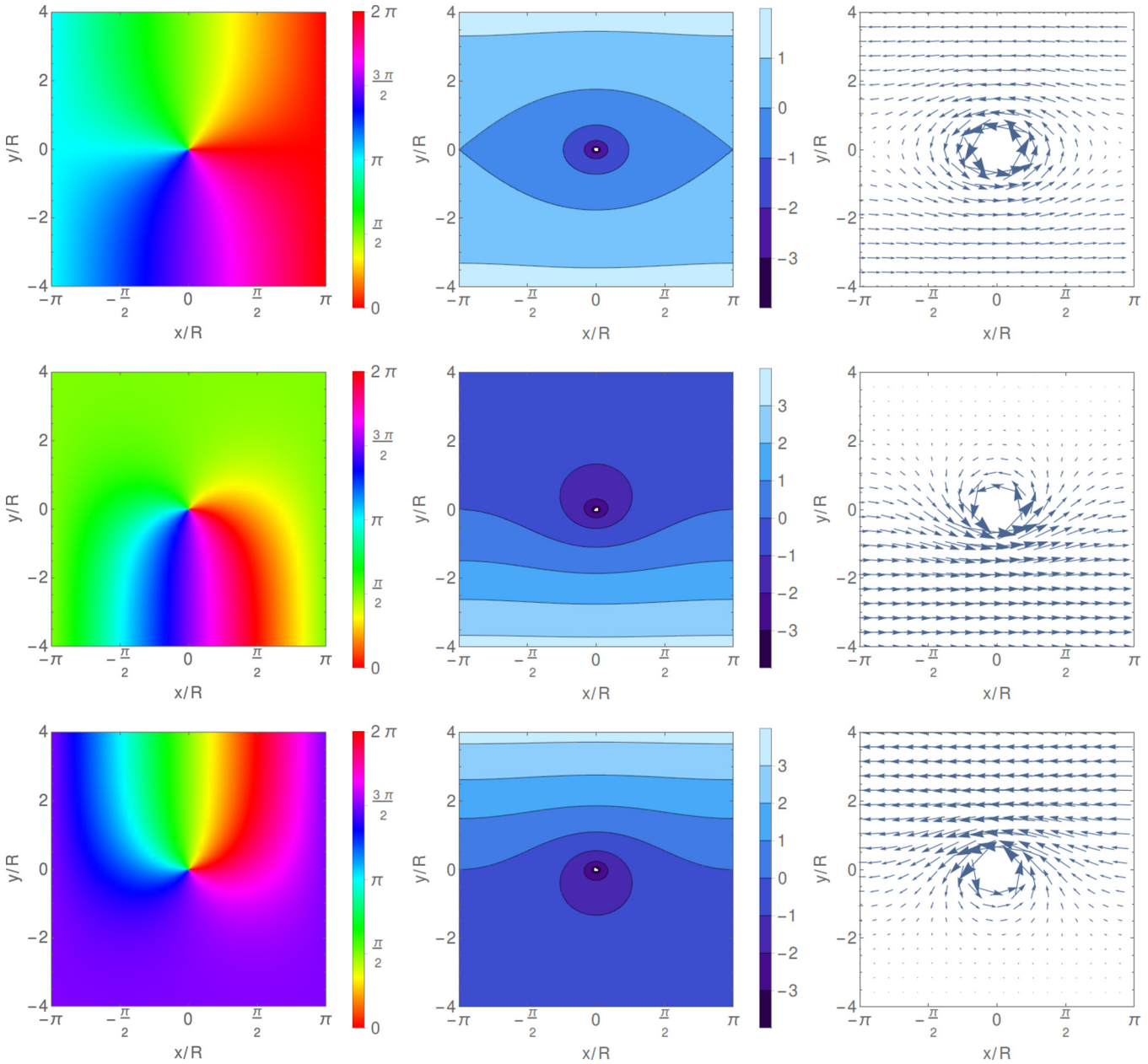

FIG. 1. Phase (left), streamlines (center), and velocity flow (right) for single point vortex on an infinite cylinder. (Top) No additional uniform flow; since the phases at $x = \pm\pi/R$ differ by π, this is not an acceptable solution for a quantum superfluid. (Middle and bottom) Additional uniform flow specified by $C = 1/2$ and $C = -1/2$, respectively (or, equivalently, $n_\uparrow = 0$ and $n_\uparrow = -1$).

from $y \to \infty$ and π flowing upward from $y \to -\infty$, as is clear from Fig. 1 (top row). Physically, the vortex on the surface can be considered the end of a vortex line in a superfluid filling the interior of the cylinder. Clearly the vortex line must come wholly from one end or the other, so that such a flux splitting is not possible. We'll see that a moving vortex indeed satisfies these conditions (for special values of the motion).

More generally, the flow velocity is $\boldsymbol{v} = \hbar\nabla\Phi/M$. Hence adding a uniform flow in the $\hat{\boldsymbol{x}}$ direction will alter the phase gradient and thus alter the phase change in going around the cylinder. Specifically, consider the more general complex potential for a vortex located at $x_0 = 0$ on the cylinder,

$$F(z) = \ln\left[\sin\left(\frac{z}{2R}\right)\right] + i\,C\,\frac{z}{R}, \tag{7}$$

where C is a dimensionless real constant. The additional uniform velocity is $(\hbar/MR)\,C\hat{\boldsymbol{x}}$. As a result, the previous expression for Φ acquires the additional term Cx/R. The additional net phase change on going once around the cylinder is $2\pi C$. Thus merely adjusting the value C can yield any desired phase change; for example, the choice $C = 1/2$ would give zero total phase change for $y > 0$ and 2π total phase change for $y < 0$. In essence, this behavior is simply the hydrodynamic analog of the familiar Bohm-Aharonov effect. Alternatively, it represents a sort of gauge freedom to alter the phase.

Figure 1 (middle and bottom) shows the phase pattern for a single positive point vortex with additional flow velocity $C = \pm 1/2$. These choices ensure that the lines of constant

phase all collect into the lower (upper) part of the cylinder for $C = 1/2\,(-1/2)$ leaving the fluid asymptotically at rest in the upper (lower) end of the cylinder. In these special cases, the net change in phase upon once encircling the cylinder now will be 0 or $\pm 2\pi$, merely by counting the phase lines crossing the path. Note that the two solutions may be mapped onto each other by a rotation of 180°, which effectively interchanges the two ends of the cylinder. Evidently, quantum mechanics requires that the phase lines from a single vortex on a cylinder must flow to $\pm\infty$ in multiples of 2π to ensure that the condensate wave function is single valued.

To clarify these questions, consider a single positive vortex on a cylinder at the origin. Integrate in a positive sense the hydrodynamic fluid velocity around a closed rectangular contour (namely the circulation) with vertical sides at $x = \mp\pi R$. Clearly, the contributions of these vertical sides cancel because of the periodicity of the flow velocity. In addition, the circulation integral will be 0 if the horizontal parts do not enclose the vortex, and 2π if the horizontal parts do enclose the vortex. For $C = 0$ (namely no external flow), the top and bottom parts each contribute π to the dimensionless circulation. If $C \neq 0$, the contributions of the top and bottom parts each shift linearly in such a way that the net circulation is unchanged. In particular, for $C = n_\uparrow + \frac{1}{2}$ with $n_\uparrow$ an integer that specifies the quantum of circulation on the horizontal path above the vortex, each horizontal part contributes a multiple of 2π.

The additional uniform flow means that the vortex now moves uniformly around the cylinder with quantized velocity, required to satisfy the quantum-mechanical condition that the condensate wave function be single valued. For any complex velocity function $F'(z)$ that contains a vortex at some point z_0, the following limit gives the complex velocity of that vortex as

$$\dot{\boldsymbol{y}}_0 + i\dot{\boldsymbol{x}}_0 = \frac{\hbar}{M}\lim_{z\to z_0}\left[F'(z) - \frac{1}{z - z_0}\right]. \tag{8}$$

In the present case, this expression simply reproduces the previous result that the vortex moves with the local uniform flow velocity. For $C = 0$ with no applied flow, any particular vortex remains at rest, either from this mathematical treatment or more physically by noting that the induced flow at any particular vortex cancels because of the left-right symmetry of the one-dimensional periodic array.

Focus on the two simplest cases with $C = \pm 1/2$, in which case the flow vanishes as $y \to \pm\infty$ [see Fig. 1 (middle and bottom)]. The corresponding complex potential becomes

$$F_\pm(z) = \ln\left[\sin\left(\frac{z}{2R}\right)\right] \pm \frac{iz}{2R} = \ln(e^{\pm iz/R} - 1) + \text{const.} \tag{9}$$

Apart from the additive constant, this complex potential is just that considered by Ho and Huang [12] as the two possible conformal transformations from a plane to a cylinder (corresponding to the choice $\pm i$). This connection clarifies the special role of the two values $C = \pm 1/2$. We consider this point in detail in Appendix A.

B. Stream function for one vortex on a cylinder

As noted in Sec. I, the stream function $\chi(\boldsymbol{r}) = \mathrm{Re}F(z)$ provides a clear picture of the hydrodynamic flow through its contour plots. In the present case, $\chi(\boldsymbol{r})$ is a little intricate, which illustrates a principal advantage of this complex formalism. Specifically, the stream function for one vortex on the surface of a cylinder of radius R is

$$\begin{aligned}\chi(\boldsymbol{r}) &= \mathrm{Re}\left\{\ln\left[\sin\left(\frac{z}{2R}\right)\right] + iC\frac{z}{R}\right\}\\ &= \frac{1}{2}\ln\left|\sin\left(\frac{x+iy}{2R}\right)\right|^2 - C\,\frac{y}{R}.\end{aligned} \tag{10}$$

Familiar complex trigonometric identities give

$$\begin{aligned}\chi(\boldsymbol{r}) &= \frac{1}{2}\ln\left[\sin^2\left(\frac{x}{2R}\right) + \sinh^2\left(\frac{y}{2R}\right)\right] - C\,\frac{y}{R}\\ &= \frac{1}{2}\ln\left[\frac{1}{2}\cosh\left(\frac{y}{R}\right) - \frac{1}{2}\cos\left(\frac{x}{R}\right)\right] - C\,\frac{y}{R},\end{aligned} \tag{11}$$

where each form is useful in different contexts.

This stream function has the proper periodicity in x and reduces to the result $\frac{1}{2}\ln[(x^2+y^2)/4R^2] - Cy/R = \ln(r/2R) - Cy/R$ for a single vortex at the origin when $r \ll R$. In contrast, for $|y| \gg R$, the stream function has the very different and asymmetric behavior $\chi(\boldsymbol{r}) \approx |y|/(2R) - Cy/R$, independent of x. Correspondingly, $\boldsymbol{\nabla}\chi(\boldsymbol{r}) \approx \hat{\boldsymbol{y}}\,[\mathrm{sgn}(y)/(2R) - C/R]$ in this limit, and the hydrodynamic flow velocity reduces to a uniform flow (from C) plus an antisymmetric uniform flow: $\boldsymbol{v}(\boldsymbol{r}) = (\hbar/M)\,\hat{\boldsymbol{n}} \times \boldsymbol{\nabla}\chi(\boldsymbol{r}) \approx -\hat{\boldsymbol{x}}\,[(\hbar/2MR)\,\mathrm{sgn}(y) - \hbar C/MR]$.

To understand this asymptotic behavior, consider the induced flow of the corresponding infinite one-dimensional array of positive vortices in the plane (for simplicity, take $C = 0$). Close to each vortex, the flow circulates around that vortex in the positive sense, but for $|y| \gtrsim \pi R$, the combined flow instead resembles that of a "vortex sheet" (see Sec. 151 of [1]). Specifically, a vortex sheet arises when the transverse velocity has a discontinuity. For example, consider the antisymmetric flow field $\boldsymbol{v} = -v_0\,\hat{\boldsymbol{x}}\,\mathrm{sgn}(y)$. Here, the vorticity is $\boldsymbol{\nabla}\times\boldsymbol{v} = 2v_0\,\delta(y)\,\hat{\boldsymbol{z}}$, which follows either by direct differentiation or with Stokes's theorem. In particular, the asymptotic flow from a periodic array of positive unit vortices along the x axis with spacing $2\pi R$ approximates a vortex sheet with $v_0 = \hbar/(2MR)$.

Evidently, the hydrodynamic flow for a single vortex on a cylinder is considerably more complicated than that for a single vortex in the plane. Note that the hydrodynamic flow arises from an analytic function $F(z)$, so that $\chi(\boldsymbol{r})$ and $\Phi(\boldsymbol{r})$ both satisfy Laplace's equation (apart from the local singularity associated with the vortex). Such a two-dimensional function cannot be periodic in both directions. Instead, the sum of the curvatures associated with x and y must vanish, so that the solution necessarily decays exponentially for large $|y|$ (in this case, to a nonzero constant), as seen here from the hyperbolic functions in $\Phi(\boldsymbol{r})$ and $\chi(\boldsymbol{r})$.

In Fig. 1 (top middle) we show a contour plot of the stream function $\chi(\boldsymbol{r})$ for a single vortex on the surface of a cylinder with $C = 0$. Lamb [1] has a similar figure in Sec. 156. As expected, the streamlines on the cylindrical surface exhibit both the periodicity in x and the exponential decay of the motion in

the $\pm y$ direction with the characteristic length $\sim R$. Note the occurrence of two topologically different types of trajectories. This phase plot resembles that of a simple pendulum, which reflects the similar canonical roles of x, y for a vortex and x, p for a pendulum. Here, the separatrix is parametrized by $\chi(\boldsymbol{r}) = 0$, namely by $\sin^2(x/2R) + \sinh^2(y/2R) = 1$. Inside the closed curves of the separatrix, the flow circulates around the vortex and its periodic images. Outside the separatrix, the flow continues in one direction, like a pendulum with large energy. In the present hydrodynamic context, streamlines inside the separatrix correspond to "libration" of the pendulum and encircle the vortex with zero winding number around the cylinder. Otherwise, streamlines correspond to "rotation" of the pendulum. They do not encircle the vortex but have winding number ∓ 1 around the cylinder, depending on the value of $-\mathrm{sgn}(y)$.

With standard trigonometric identities, it is not hard to find the hydrodynamic flow velocity induced by the single positive vortex at the origin on the surface of a cylinder (here, for simplicity, we take $C = 0$):

$$\begin{aligned}\boldsymbol{v}(\boldsymbol{r}) &= \frac{\hbar}{2MR}\,\frac{-\hat{\boldsymbol{x}}\sinh(y/R) + \hat{\boldsymbol{y}}\sin(x/R)}{\cosh(y/R) - \cos(x/R)} \\ &= \frac{\hbar}{2MR}\,\hat{\boldsymbol{n}} \times \left[\frac{\hat{\boldsymbol{x}}\sin(x/R) + \hat{\boldsymbol{y}}\sinh(y/R)}{\cosh(y/R) - \cos(x/R)}\right] \\ &= \frac{\hbar}{M}\,\hat{\boldsymbol{n}} \times \nabla\chi(\boldsymbol{r}). \end{aligned} \tag{12}$$

The resulting flow pattern is shown in Fig. 1 (top right). For $|x| \ll R$ and $|y| \ll R$, the hydrodynamic flow field reduces to the familiar expression $\boldsymbol{v}(x,y) \approx (\hbar/M)\,\hat{\boldsymbol{n}} \times \boldsymbol{r}/r^2 = (\hbar/Mr)\,\hat{\boldsymbol{\phi}}$, which falls off inversely with the distance from the vortex in all directions. For large $|y|/R$ on a cylinder, in contrast, the flow velocity reduces to a constant $\boldsymbol{v}(x,y) \approx -(\hbar/2MR)\,\hat{\boldsymbol{x}}\,\mathrm{sgn}(y)$. In this region the periodicity around the cylinder dominates the flow pattern, rather than the single vortex.

III. MULTIPLE VORTICES ON A CYLINDER

It is now straightforward to generalize the previous discussion to the case of N vortices on an infinite cylinder, each located at complex position z_j and with charge $q_j = \pm 1$ $(j = 1, \ldots, N)$. As in electrostatics, the complex potential for multiple vortices on the cylindrical surface is simply the sum of the complex potentials of the individual vortices, always with the option of adding a uniform flow of the form iCz/R. For an even number of vortices, however, this term is unnecessary.

$$F^{(N)}(z) = \sum_{j=1}^{N} q_j F(z - z_j) = \sum_{j=1}^{N} q_j \ln\left[\sin\left(\frac{z - z_j}{2R}\right)\right]. \tag{13}$$

The corresponding velocity potential $\Phi^{(N)}(\boldsymbol{r})$ and stream function $\chi^{(N)}(\boldsymbol{r})$ are the imaginary and real parts of $F^{(N)}(z)$ and need not be given explicitly.

A. Induced motion of two vortices on a cylinder

As noted at the end of Sec. II A, in the absence of external flow a single vortex on a cylinder remains stationary. Consequently, the motion of each vortex arises only from the presence of the other vortex. Equation (8) immediately gives the complex velocity of the first vortex,

$$\dot{y}_1 + i\dot{x}_1 = \frac{\hbar}{MR}\,\frac{q_2}{2}\,\cot\left(\frac{z_1 - z_2}{2R}\right), \tag{14}$$

and similarly,

$$\dot{y}_2 + i\dot{x}_2 = -\frac{\hbar}{MR}\,\frac{q_1}{2}\,\cot\left(\frac{z_1 - z_2}{2R}\right). \tag{15}$$

It is now helpful to introduce the vector notation used in Sec. II A. For two vortices at $\boldsymbol{r}_1$ and $\boldsymbol{r}_2$, let $\boldsymbol{R}_{12} = \frac{1}{2}(\boldsymbol{r}_1 + \boldsymbol{r}_2)$ be the centroid and $\boldsymbol{r}_{12} = \boldsymbol{r}_1 - \boldsymbol{r}_2$ be the relative position (note that the vector $\boldsymbol{r}_{12}$ runs from 2 to 1). As a result [compare Eq. (12)], we find the appropriate dynamical equations,

$$\dot{\boldsymbol{R}}_{12} = \frac{\hbar}{MR}\left(\frac{q_1 - q_2}{4}\right)\left[\frac{\hat{\boldsymbol{x}}\sinh(y_{12}/R) - \hat{\boldsymbol{y}}\,\sin(x_{12}/R)}{\cosh(y_{12}/R) - \cos(x_{12}/R)}\right],$$

and

$$\dot{\boldsymbol{r}}_{12} = \frac{\hbar}{MR}\left(\frac{q_1 + q_2}{4}\right)\left[\frac{-\hat{\boldsymbol{x}}\sinh(y_{12}/R) + \hat{\boldsymbol{y}}\,\sin(x_{12}/R)}{\cosh(y_{12}/R) - \cos(x_{12}/R)}\right].$$

B. Two vortices with opposite signs (vortex dipole)

When $q_1 = 1$ and $q_2 = -1$, the vortex dipole moves with no internal rotation $\dot{\boldsymbol{r}}_{12} = \boldsymbol{0}$ (so that x_{12} and y_{12} remain constant, simplifying the subsequent dynamics). Furthermore, the centroid moves with uniform translational velocity,

$$\begin{aligned}\dot{\boldsymbol{R}}_{12} &= \frac{\hbar}{2MR}\left[\frac{\hat{\boldsymbol{x}}\sinh(y_{12}/R) - \hat{\boldsymbol{y}}\,\sin(x_{12}/R)}{\cosh(y_{12}/R) - \cos(x_{12}/R)}\right] \\ &= -\frac{\hbar}{M}\,\hat{\boldsymbol{n}} \times \nabla\chi(\boldsymbol{r}_{12}), \end{aligned} \tag{16}$$

at fixed x_{12} and y_{12}. Several limits are of interest.

(1.) If $|x_{12}| \ll R$ and $|y_{12}| \ll R$, then the translational velocity is the same as that for a vortex dipole on a plane:

$$\dot{\boldsymbol{R}}_{12} = \frac{\hbar}{M}\,\frac{\hat{\boldsymbol{x}}\,y_{12} - \hat{\boldsymbol{y}}\,x_{12}}{x_{12}^2 + y_{12}^2} = -\frac{\hbar}{M}\,\frac{\hat{\boldsymbol{n}} \times \boldsymbol{r}_{12}}{r_{12}^2}. \tag{17}$$

Detailed analysis confirms that the vortex dipole moves in the direction of the flow between their centers.

(2.) If $|y_{12}| \gg R$, then the ratio of hyperbolic functions leaves only the $\hat{\boldsymbol{x}}$ component, with $\dot{\boldsymbol{R}}_{12} = (\hbar/2MR)\,\hat{\boldsymbol{x}}\,\mathrm{sgn}(y_{12})$. This value reflects the hydrodynamic flow from a periodic array of vortices, as mentioned near the end of Sec. II B. In this limit, the vortex dipole will circle the cylinder in a time $4\pi MR^2/\hbar$. Note that this motion is the same as that induced for one vortex with $C = \pm 1/2$, discussed in Sec. II A. Hence the additional induced motion of a single vortex on an infinite cylinder can alternatively be thought to arise from a phantom negative vortex placed at $y_0' \to \mp\infty$, corresponding to $C = \pm 1/2$.

As an example, Fig. 2 shows the hydrodynamic streamlines for various orientations of the relative position $z_1 - z_2$. Specifically, we plot the corresponding stream function χ for

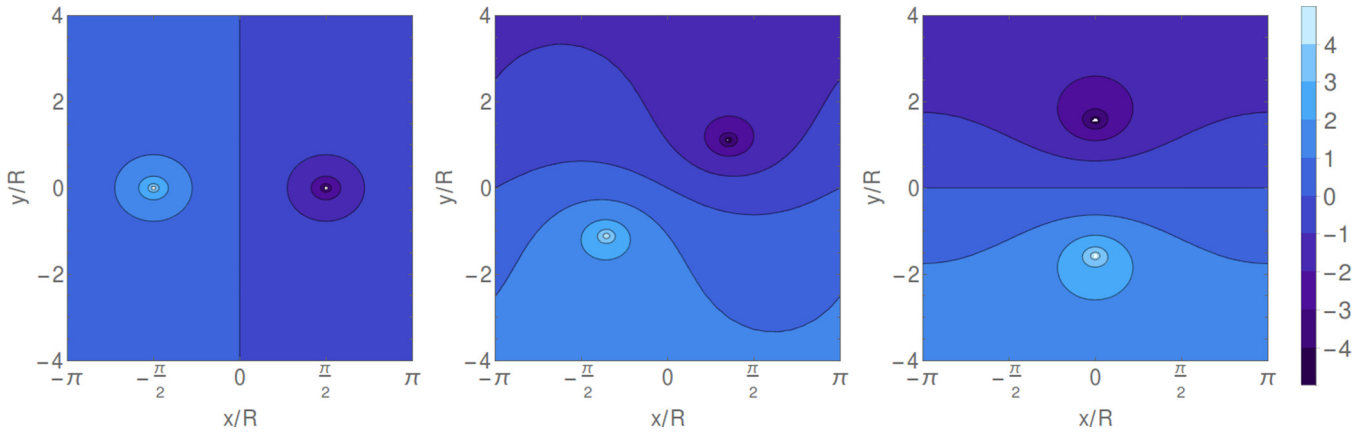

FIG. 2. Hydrodynamic streamlines for vortex dipole $q_1 = -q_2 = 1$ on a cylinder of radius R, for various orientations of the dipole axis.

three typical cases: $y_{12} = 0$ with motion along $-\hat{\boldsymbol{y}}$, $x_{12} = y_{12}$, with motion along $\hat{\boldsymbol{x}} - \hat{\boldsymbol{y}}$, and $x_{12} = 0$ with motion along $\hat{\boldsymbol{x}}$.

C. Two vortices with same signs

In the case of two positive vortices ($q_1 = q_2 = 1$), it follows immediately that $\dot{\boldsymbol{R}}_{12}$ vanishes, so that the centroid of the two vortices remains fixed. In contrast, the relative vector obeys the nontrivial equation of motion,

$$\begin{aligned}\dot{\boldsymbol{r}}_{12} &= \dot{x}_{12}\,\hat{\boldsymbol{x}} + \dot{y}_{12}\,\hat{\boldsymbol{y}} \\ &= \frac{\hbar}{M}\left[\frac{-\hat{\boldsymbol{x}}\,\sinh(y_{12}/R) + \hat{\boldsymbol{y}}\,\sin(x_{12}/R)}{\cosh(y_{12}/R) - \cos(x_{12}/R)}\right] \\ &= \frac{\hbar}{M}\hat{\boldsymbol{n}} \times \boldsymbol{\nabla}\chi(\boldsymbol{r}_{12}) = \boldsymbol{v}(\boldsymbol{r}_{12}). \end{aligned} \tag{18}$$

Unlike the case of opposite charges (where $\dot{\boldsymbol{r}}_{12}$ remains fixed), the relative vector $\boldsymbol{r}_{12}$ now becomes time dependent. In fact, the last form given above shows that the motion of the two positive vortices precisely follows the hydrodynamic flow velocity of a single vortex $\boldsymbol{v}(x_{12}, y_{12})$. Hence the streamlines in Fig. 1 (central column) completely characterize the motion. Several cases are of interest.

(1.) If $x_{12}^2 + y_{12}^2 \ll R^2$, then the two positive vortices simply circle in the positive sense around their common center $\boldsymbol{R}_{12}$. The curvature of the surface is irrelevant and the motion is the same as on a flat plane.

(2.) If $\sin^2(x_{12}/2R) + \sinh^2(y_{12}/2R) < 1$, the two vortices execute closed orbits in the positive sense around their common center $\boldsymbol{R}_{12}$, but the general orbits are not circular [by definition, they remain inside the separatrix in Fig. 1 (top row, central column)].

(3.) If $\sin^2(x_{12}/2R) + \sinh^2(y_{12}/2R) > 1$, the two vortices move in opposite directions, executing periodic closed orbits around the cylinder with unit winding number. The upper vortex moves monotonically to the left and the lower vortex moves monotonically to the right, as seen in Fig. 1 (top row, central column) (they remain outside the separatrix).

(4.) For relatively large $|y_{12}|/R$, an expansion of the above equation yields the approximate form,

$$\begin{aligned}\dot{\boldsymbol{r}}_{12} \approx \frac{\hbar}{MR}\{&-\mathrm{sgn}(y_{12}/R)[1 - 2\cos(x_{12}/R)\,e^{-|y_{12}|/R}]\,\hat{\boldsymbol{x}} \\ &+ 2\sin(x_{12}/R)\,e^{-|y_{12}|/R}\,\hat{\boldsymbol{y}}\}. \end{aligned} \tag{19}$$

Asymptotically for $|y_{12}| \gg R$, the variable x_{12} varies linearly in time. The leading correction to this uniform horizontal motion is a small periodic modulation for both $\hat{\boldsymbol{x}}$ and $\hat{\boldsymbol{y}}$ components.

IV. ENERGY OF TWO VORTICES

The stream function $\chi(\boldsymbol{r})$ provides the hydrodynamic flow velocity $\boldsymbol{v}(\boldsymbol{r})$ through Eq. (1), which is its usual role. As shown below, however, the stream function also determines the interaction energy E_{12} between two point vortices through Eq. (23). The analogous electrostatic situation is familiar in that the electrostatic potential gives both the electric field from a single point charge and the interaction energy of two point charges. For electrostatics, this connection follows directly as the work done to bring the second charge in from infinity. For vortices, however, such an argument is less clear, since vortices do not act like Newtonian particles and obey first-order equations of motion. Hence we present a straightforward analysis that gives the interaction energy E_{12} of two vortices by integrating the kinetic-energy density, which is proportional to the squared velocity field. This approach is clearly analogous to finding the electrostatic interaction energy of two charges by integrating the electrostatic-energy density, which is proportional to the squared electrostatic field.

In the present model, the total energy of two vortices at $\boldsymbol{r}_j$ ($j = 1,2$) with unit charge $q_j = \pm 1$ is the spatial integral of the kinetic-energy density,

$$\begin{aligned}E_{\mathrm{tot}} &= \tfrac{1}{2}nM\int d^2r[q_1\,\boldsymbol{v}(\boldsymbol{r} - \boldsymbol{r}_1) + q_2\,\boldsymbol{v}(\boldsymbol{r} - \boldsymbol{r}_2)]^2 \\ &= \tfrac{1}{2}nM\int d^2r\big[|\boldsymbol{v}(\boldsymbol{r} - \boldsymbol{r}_1)|^2 + |\boldsymbol{v}(\boldsymbol{r} - \boldsymbol{r}_2)|^2 \\ &\quad + 2q_1q_2\,\boldsymbol{v}(\boldsymbol{r} - \boldsymbol{r}_1)\cdot\boldsymbol{v}(\boldsymbol{r} - \boldsymbol{r}_2)\big], \end{aligned} \tag{20}$$

over the surface of the cylinder. Here, $\boldsymbol{v}(\boldsymbol{r})$ is the hydrodynamic velocity field of a single positive unit vortex at the origin, n is the two-dimensional number density, and M is the atomic mass.

A. Interaction energy

As noted in Secs. II A and II B, for large $|y|/R$, the asymptotic velocity field of a single vortex on a cylinder is uniform. Hence the kinetic energy of any single vortex diverges

linearly as the upper and lower integration boundaries on the cylinder become large (namely $|y| = Y \to \infty$). As a result, each term in the above kinetic energy of two vortices on a cylinder separately diverges. The only case with a finite total kinetic energy is the vortex dipole with (say) $q_1 = 1$ and $q_2 = -1$, since the two asymptotic hydrodynamic velocity flow fields then cancel.

It is convenient to use the stream function to characterize the local fluid velocity of the jth vortex: $\boldsymbol{v}(\boldsymbol{r} - \boldsymbol{r}_j) = (\hbar/M)\hat{\boldsymbol{n}} \times \nabla\chi_j$, where $\chi_j = \chi(\boldsymbol{r} - \boldsymbol{r}_j)$ [compare Eq. (1)]. The operation $\hat{\boldsymbol{n}}\times$ simply rotates the following vector through $\pi/2$ and we find

$$\begin{aligned} E_{\rm tot} &= \frac{n\hbar^2}{2M}\int d^2r (q_1\nabla\chi_1 + q_2\nabla\chi_2)^2 \\ &= \frac{n\hbar^2}{2M}\int d^2r \{\nabla\cdot[(\chi_1 + q_1q_2\chi_2)\nabla(\chi_1 + q_1q_2\chi_2)] \\ &\quad - \chi_1\nabla^2\chi_1 - \chi_2\nabla^2\chi_2 - q_1q_2(\chi_1\nabla^2\chi_2 + \chi_2\nabla^2\chi_1)\}. \end{aligned} \tag{21}$$

We follow de Gennes's argument for type-II superconductors [13], but the analysis is also familiar from classical electrostatics. Here, the two-dimensional surface integral runs over the region $-\pi R \leqslant x \leqslant \pi R$ and $-Y \leqslant y \leqslant Y$, where $Y \to \infty$.

The first term above involves the divergence of the total derivative $\frac{1}{2}\nabla(\chi_1 + q_1q_2\chi_2)^2$, and the divergence theorem reduces it to an integral on the boundary with outward unit normals. The contributions from the vertical parts at $x = \pm\pi R$ cancel because the integrand is periodic with period $2\pi R$. In general, the contributions from the horizontal parts at $y = \pm Y$ separately diverge linearly, except for the special case of a vortex dipole with $q_1q_2 = -1$. The relevant quantity is $\frac{1}{2}\partial_y(\chi_1 - \chi_2)^2$ for large $|y|$. Equation (11) gives (here we take $C = 0$ since the system is neutral)

$$\begin{aligned} \chi_1 - \chi_2 &= \frac{1}{2}\ln\left[\frac{\sin^2[(x-x_1)/2R] + \sinh^2[(y-y_1)/2R]}{\sin^2[(x-x_2)/2R] + \sinh^2[(y-y_2)/2R]}\right] \\ &\approx \frac{|y-y_1| - |y-y_2|}{2R} + \cdots \\ &= \text{constant} + \cdots \text{ for } |y| \to \infty, \end{aligned} \tag{22}$$

where the corrections are exponentially small for large $|y|$. It is now clear that each horizontal contribution vanishes for the present case of a vortex dipole, reflecting the overall charge neutrality.

It remains to evaluate the second line of Eq. (21). We already noted that $\nabla^2\chi_j = \nabla^2\chi(\boldsymbol{r} - \boldsymbol{r}_j) = 2\pi\delta^{(2)}(\boldsymbol{r} - \boldsymbol{r}_j)$, and the interaction energy (the terms involving the cross product of χ_1 and χ_2) thus becomes

$$E_{12} = -(2\pi n\hbar^2/M)\, q_1q_2\, \chi(\boldsymbol{r}_{12}), \tag{23}$$

for general choice of q_1q_2. The dynamics of two vortices involves gradient operations like $\nabla_1 E_{12}$, so that any divergent constant becomes irrelevant (alternatively, we can redefine the zero of the energy). As in Eq. (7) of [7], it is convenient to take out a factor $2\pi n\hbar$, writing

$$V_{12} = -q_1q_2\,(\hbar/M)\,\chi(\boldsymbol{r}_{12}), \tag{24}$$

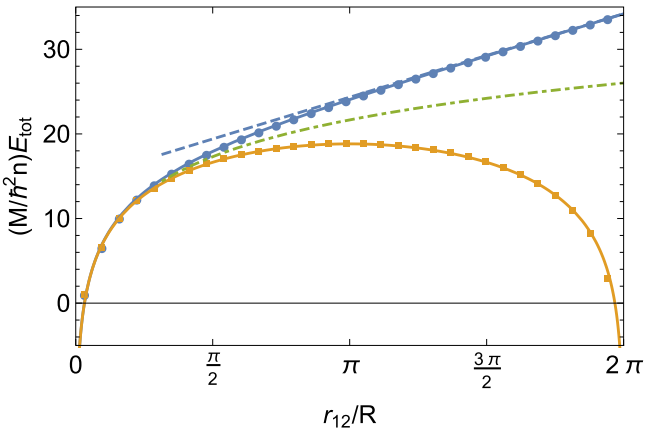

FIG. 3. Energy of a vortex dipole on an infinite cylinder, as a function of the intervortex separation r_{12}, for a dipole oriented along the axis of the cylinder and moving along the equatorial direction (dark blue), and for a vortex dipole oriented along the equator and moving along the axial direction (light orange). The vortex core size is set to $\xi = R/10$. Symbols display the numerical evaluation of Eq. (21), and solid lines show the analytical result in Eq. (27). The dot-dashed green line is the usual result on the plane, $E_{\rm tot} = (2\pi\hbar^2 n/M)[\ln(r_{12}/2R) + \ln(2R/\xi)]$, and the dashed line is the asymptotic behavior for large axial separation $y_{12} \gg R$, $E_{\rm tot} = (2\pi\hbar^2 n/M)[y_{12}/(2R) + \ln(R/\xi)]$.

which properly reduces to $q_1q_2\,(\hbar/M)\ln(2R/r_{12})$ for small intervortex separation.

B. Self-energy of one vortex

Equation (21) also contains two self-energy terms, one for each vortex. Consider a single vortex 1 at the origin with self-energy,

$$\begin{aligned} E_1 &= \frac{n\hbar^2}{2M}\int d^2r\, \nabla\chi(\boldsymbol{r})\cdot\nabla\chi(\boldsymbol{r}) \\ &= \frac{n\hbar^2}{2M}\int d^2r\, \{\nabla\cdot[\chi(\boldsymbol{r})\nabla\chi(\boldsymbol{r})] - \chi(\boldsymbol{r})\nabla^2\chi(\boldsymbol{r})\}. \end{aligned} \tag{25}$$

A heuristic approach for the self-energy terms (those involving $-\chi_j\nabla^2\chi_j$) in Eq. (21) is to cut off the singularity at the small core radius ξ, which gives

$$E_1 = \frac{\pi n\hbar^2}{M}\ln\left(\frac{2R}{\xi}\right). \tag{26}$$

The finite total energy of a vortex dipole is simply the sum of the interaction energy and the two self-energies,

$$E_{\rm tot} = E_{12} + 2E_1 = \frac{2\pi n\hbar^2}{M}\left[\chi(\boldsymbol{r}_{12}) + \ln\left(\frac{2R}{\xi}\right)\right]. \tag{27}$$

Note that this total vortex energy reduces to the familiar $\ln(r_{12}/\xi)$ for small r_{12}. Otherwise it has a very different form and grows linearly for $|y_{12}| \gg R$ (see Fig. 3). This interaction energy was already discussed in previous studies of Berezinskii-Kosterlitz-Thouless behavior for a thin cylindrical film [14], and of vortex dipoles on capped cylinders [9].

This analysis holds whenever a stream function describes the flow, even in the presence of boundaries when $\chi(\boldsymbol{r},\boldsymbol{r}_j)$ in-

volves two separate variables. Here, it yields the general result,

$$E_{\rm tot} = -\frac{\pi n\hbar^2}{M}\sum_{j,k=1}^{2} q_j q_k \chi(\boldsymbol{r}_j,\boldsymbol{r}_k), \tag{28}$$

augmented by the cutoff at ξ when $j = k$.

As seen below, this approach also works for vortices on a finite cylinder, where the method of images gives the complex potential (see Sec. V). Finally, it describes the energy of point vortices in a planar annulus [11] (see Appendix B).

C. Vortex motion as response to applied force

The modified interaction energy $V_{12}(\boldsymbol{r}_{12})$ in Eq. (24) allows us to rewrite the two vector dynamical equations near the start of Sec. III A as follows:

$$q_1\dot{\boldsymbol{r}}_1 = -\hat{\boldsymbol{n}}\times\boldsymbol{\nabla}_1 V_{12} \quad \text{and} \quad q_2\dot{\boldsymbol{r}}_2 = -\hat{\boldsymbol{n}}\times\boldsymbol{\nabla}_2 V_{12}. \tag{29}$$

We can interpret the quantity $\boldsymbol{F}_1 = -\boldsymbol{\nabla}_1 V_{12}$ as the force that vortex 2 exerts on vortex 1, and similarly with $\boldsymbol{F}_2 = -\boldsymbol{\nabla}_2 V_{12} = -\boldsymbol{F}_1$, where the last relation follows because V_{12} depends only on the difference of the coordinates.

In this way, the dynamical equations take the intuitive form (see Sec. III of [7]),

$$q_1\dot{\boldsymbol{r}}_1 = \hat{\boldsymbol{n}}\times\boldsymbol{F}_1 \quad \text{and} \quad q_2\dot{\boldsymbol{r}}_2 = \hat{\boldsymbol{n}}\times\boldsymbol{F}_2 = -\hat{\boldsymbol{n}}\times\boldsymbol{F}_1. \tag{30}$$

Hence a vortex moves perpendicular to the applied force, which is often called the Magnus effect. Equivalently, we can introduce the "Magnus force" $\boldsymbol{F}_j^M = q_j\hat{\boldsymbol{n}}\times\dot{\boldsymbol{r}}_j$, and the dynamical equation then becomes $\boldsymbol{F}_j^M + \boldsymbol{F}_j = \boldsymbol{0}$. These equations concisely express two-dimensional vortex dynamics in a general form, applying not only to motion on a plane but also on a cylinder.

D. Energy of multiple vortex dipoles

As seen in Sec. III, the stream function for a set of N vortices on an infinite cylinder is the sum of individual terms $\chi = \sum_{i=1}^{N}\chi_i$, where we assume N is even. The total kinetic energy of the vortices is proportional to $\int d^2r|\boldsymbol{\nabla}\chi|^2$ over the area of the cylinder. This behavior is completely analogous to the electrostatic energy for two-dimensional point charges on a cylindrical surface, since the electrostatic energy is proportional to the integral $\int d^2r|\boldsymbol{E}|^2$, and $\boldsymbol{E}$ is the (negative) gradient of the electrostatic potential $\mathcal{P}$. Furthermore, the total electrostatic potential is a sum of contributions $\mathcal{P}_j$ from each charge, like the similar structure of the total χ. Finally, Eq. (4) shows that the stream function χ obeys Poisson's equation with each vortex as a source, in complete analogy to the electrostatic potential $\mathcal{P}$ which also obeys Poisson's equation with the point charges as sources.

Thus, by analogy with two-dimensional electrostatics, the energy of multiple pairs of point vortices on the infinite cylinder follows immediately as the sum over all pairs plus the sum over all self-energies,

$$\begin{aligned} E_{\rm tot} &= E_{\rm int} + E_{\rm self} = \sum_{i<j}^{N} E_{ij} + \sum_{i}^{N} E_i \\ &= -\sum_{i<j}^{N} q_i q_j \frac{2\pi n\hbar^2}{M}\chi(\boldsymbol{r}_{ij}) + N\frac{\pi n\hbar^2}{M}\ln\left(\frac{2R}{\xi}\right). \end{aligned} \tag{31}$$

If the system is overall neutral, then the total energy is finite; otherwise, there are divergent constant terms that do not affect the dynamics of individual vortices. Similar divergences appear in two-dimensional electrostatics unless the total electric charge vanishes.

Equations (1), (3), and (31) together give the general dynamical equations,

$$q_k\dot{\boldsymbol{x}}_k = \frac{\partial V_{\rm int}}{\partial y_k} \quad \text{and} \quad q_k\dot{\boldsymbol{y}}_k = -\frac{\partial V_{\rm int}}{\partial x_k}, \tag{32}$$

where $V_{\rm int} = -\sum_{i<j}^{N} q_i q_j\,(\hbar/M)\chi(\boldsymbol{r}_{ij})$. Thus $V_{\rm int}$ serves as a "Hamiltonian" with canonical variables (x_k, y_k) that determines the motion of all the vortices.

V. SINGLE VORTEX ON A CYLINDER OF FINITE LENGTH

As seen in the previous sections, the complex potential generated by a single positive vortex located at the origin of a cylinder with radius R and of infinite length, is

$$F(z) = \ln\left[\sin\left(\frac{z}{2R}\right)\right]. \tag{33}$$

The corresponding solution on a cylinder with finite length L (with $0 \leqslant y \leqslant L$) follows with the method of images. Consider a physical vortex located at $z_0 = (x_0 + iy_0)$ with $0 < y_0 < L$. Reflect the potential of the unbounded solution along the planes $y = iL$ and $y = 0$ and reverse the charge of successive image vortices. This procedure creates an infinite set of positive vortices at positions $z_{(n,+)} = z_0 + 2inL$ and negative vortices at $z_{(n,-)} = z_0^* + 2inL$. We find

$$F_L(z) = \sum_{n\in\mathbb{Z}}\left\{\ln\left[\sin\left(\frac{z - z_{(n,+)}}{2R}\right)\right] - \ln\left[\sin\left(\frac{z - z_{(n,-)}}{2R}\right)\right]\right\} = \ln\left[\prod_{n\in\mathbb{Z}}\left(\frac{\sin(z_+/R - i\beta n)}{\sin(z_-/R - i\beta n)}\right)\right], \tag{34}$$

where $z_+ = (z - z_0)/2$, $z_- = (z - z_0^*)/2$, and $\beta = L/R$.

Examine the infinite product in Eq. (34) in detail:

$$\begin{aligned} \prod_{n\in\mathbb{Z}}\left(\frac{\sin(z_+/R - i\beta n)}{\sin(z_-/R - i\beta n)}\right) &= \frac{\sin(z_+/R)}{\sin(z_-/R)}\prod_{n=1}^{\infty}\left(\frac{\sin(z_+/R - i\beta n)\sin(z_+/R + i\beta n)}{\sin(z_-/R - i\beta n)\sin(z_-/R + i\beta n)}\right) \\ &= \frac{\sin(z_+/R)}{\sin(z_-/R)}\prod_{n=1}^{\infty}\left(\frac{2\cos(2z_+/R) - q^{2n} - q^{-2n}}{2\cos(2z_-/R) - q^{2n} - q^{-2n}}\right) = \frac{\vartheta_1(z_+/R,q)}{\vartheta_1(z_-/R,q)}, \end{aligned} \tag{35}$$

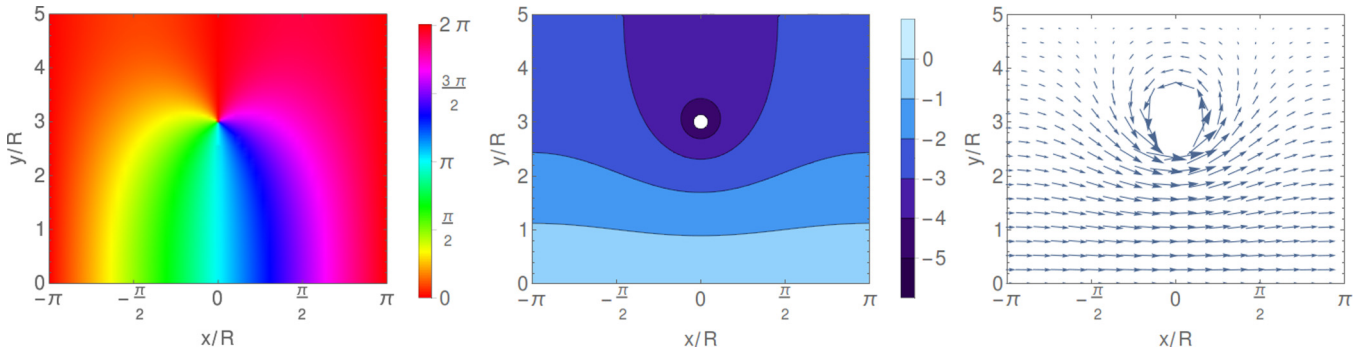

FIG. 4. Single vortex on a finite cylinder of length $L = 5R$, located at $y_0 = 3R$. From left to right, plots show the phase Φ, the stream function χ, and the velocity field $\boldsymbol{v}$.

where $q = e^{-\beta} = e^{-L/R}$. Here, $\vartheta_1(z,q)$ denotes the first Jacobi ϑ function, defined by either its product form or its series form [10],

$$\vartheta_1(z,q) = 2q^{1/4}\sin(z)\prod_{n=1}^{\infty}(1-q^{2n})(1-2q^{2n}\cos(2z)+q^{4n})$$
$$= 2\sum_{n=0}^{\infty}(-1)^n q^{(n+1/2)^2}\sin[(2n+1)z]. \quad (36)$$

This function has simple zeros at the complex points $z = m\pi + n\pi\tau$, where $m,n \in \mathbb{Z}$ and τ is a complex number with positive imaginary part. In addition, the parameter $q = e^{i\pi\tau}$ obeys the condition $|q| < 1$. Here, $\tau = i\beta/\pi = iL/\pi R$ and hence $q = e^{-L/R}$, as noted above.

The final complex potential for a vortex located at z_0 on a cylinder of length L and radius R has the relatively simple analytic form,

$$F_L(z) = \ln\left[\frac{\vartheta_1\left(\frac{z-z_0}{2R}, e^{-L/R}\right)}{\vartheta_1\left(\frac{z-z_0^*}{2R}, e^{-L/R}\right)}\right]. \quad (37)$$

Figure 4 shows the phase $\Phi(\boldsymbol{r}) = \mathrm{Im}F_L(z)$, the stream function $\chi(\boldsymbol{r}) = \mathrm{Re}F_L(z)$, and the vector velocity field $\boldsymbol{v}(\boldsymbol{r})$ obtained from $v_y + iv_x = (\hbar/M)F_L'(z)$. These plots may be compared to the analogous ones for an infinite cylinder shown in Fig. 1 (middle row).

The first Jacobi theta function $\vartheta_1(z,q)$ changes sign when $z \to z \pm \pi$, immediately proving that the phase of the wave function changes by integer multiples of 2π when $x \to x \pm 2\pi R$. In particular, the integral $\int_{-\pi R}^{\pi R} dx\ v_x$, computed at fixed y, equals 0 above the vortex ($y > y_0$), and $2\pi\hbar/M$ below ($y < y_0$), as is clear from Fig. 4 (left). Hence, the complex potential $F_L(z)$ always generates "quantum-mechanically acceptable" solutions that move uniformly around the cylinder.

By construction, the fluid is basically at rest above the vortex, and in motion below it. This result may be understood by noting that the original vortex and its image below the bottom end of the cylinder replicate a vortex dipole located at (z_0, z_0^*). In this basic "building block," the fluid flow is largely confined to the region between the two vortices and vanishes at large distances from the line (or domain wall) joining the two vortices.

Note furthermore that v_y is manifestly antisymmetric around a vertical axis passing through the vortex core [namely, $v_y(x - x_0, y) = -v_y(x_0 - x, y)$], so that its line integral along a circumference (at fixed y) vanishes. As a consequence, the angular momentum per particle on the cylinder is simply $\hbar(y_0/L)$. If angular momentum were to be "pumped" at a constant (slow) rate into the system (namely, if the cylinder were to be spun with a linearly increasing rotation frequency, or if an increasing synthetic flux pierced the surface of the cylinder, as discussed in Ref. [15]), a vortex would enter the lower rim of the cylinder and progressively spiral up the cylinder. Once the vortex reaches the upper rim and leaves the cylinder, the angular momentum per particle would increase by exactly $\hbar$. This mechanism is a direct hydrodynamic analog of the Laughlin pumping [16].

A. Velocity of the vortex core

The velocity of the vortex core follows from Eq. (8),

$$\lim_{z\to z_0}\left(F_L'(z) - \frac{1}{z-z_0}\right) = -\frac{1}{2R}\frac{\vartheta_1'(iy_0/R, e^{-L/R})}{\vartheta_1(iy_0/R, e^{-L/R})}, \quad (38)$$

where $\vartheta'(z,q)$ indicates the derivative of ϑ with respect to its variable z. This function is purely imaginary, indicating that the vortex moves solely along the $\hat{\boldsymbol{x}}$ direction, and its velocity diverges as it approaches either end of the cylinder (namely, one of the image charges), as shown in Fig. 5. If the vortex is located at the middle of the cylinder at $z_0 = x_0 + iL/2$, one may use the property $\vartheta_1'(iu/2, e^{-u}) = -i\vartheta_1(iu/2, e^{-u})$ (valid for generic real $u > 0$) to show that it moves uniformly around the cylinder with speed,

$$\dot{\boldsymbol{x}}_0 = \hbar/2MR \text{ when } y_0 = L/2, \quad (39)$$

as seen in Fig. 5. Here the rightward motion arises because we chose to pair the vortex with its image in the lower boundary of the cylinder. Had we instead used the image in the upper boundary at $z_0^* + 2iL$, the motion would have been to the left with the same magnitude. This broken symmetry is just that seen in Sec. II associated with the choice $C = \pm 1/2$.

B. Analytical limits for long and short cylinders

When $L \gg R$, the parameter q is small, so that we may approximate $\vartheta_1(z,q) \approx 2q^{1/4}\sin(z)$. For a vortex at the complex position z_0, let $z \approx z_0 + z'$, where $z' = z - z_0$ is

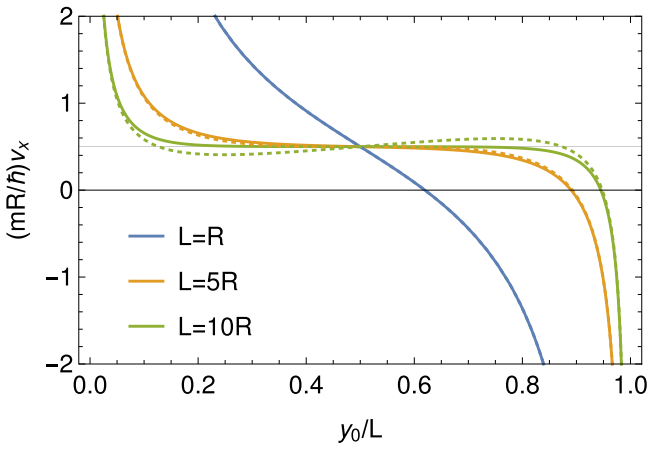

FIG. 5. Velocity of the vortex core as a function of its vertical coordinate y_0, for various cylinder lengths L (from top to bottom, on the left side, the lines represent $L = R, 5R, 10R$). The dotted lines are the approximate results, valid in the limit $L \lesssim \pi R$, obtained from Eq. (44). The blue dotted line is indistinguishable from the solid one.

small. Hence the previous $F_L(z)$ becomes

$$F_L(z) \approx \ln\left[\frac{\sin(z'/2R)}{\sin(2iy_0/2R + z'/2R)}\right], \tag{40}$$

where we assume $z_0 = iy_0$. It is convenient to take $y_0 = L/2$, placing the vortex at the center of the cylinder.

In this case, the denominator here becomes $\sin(iL/2R + z'/2R) \approx i\frac{1}{2}e^{L/2R}(1 - iz'/2R)$. As a result, we find the approximate expression,

$$F_L(z) \approx \ln\sin\left(\frac{z'}{2R}\right) + \frac{iz'}{2R} - \frac{L}{2R} - \frac{i\pi}{2} + \ln 2. \tag{41}$$

Apart from the additive constant terms, this result is precisely that found in Sec. II A for an infinite cylinder with a vortex at the origin and zero velocity flow on its (distant) upper rim.

When we have the opposite limit $L \ll R$, we may use the Jacobi imaginary transformation that relates a theta function with parameter τ to one with parameter $\tau' = -1/\tau$ [10]. Here, $\tau' = i\pi R/L$ and $q' = e^{i\pi\tau'} = e^{-\pi^2 R/L}$ is now small. The relevant transformation formula becomes

$$\vartheta_1\left(\frac{z}{R}, e^{-L/R}\right) = i\sqrt{\frac{\pi R}{L}}\, e^{-z^2/RL}\, \vartheta_1\left(\frac{z\pi}{iL}, e^{-\pi^2 R/L}\right). \tag{42}$$

In this way we find

$$F_{L\ll R}(z) = \ln\left[\frac{e^{-[(z-z_0)^2/4RL]}\,\vartheta_1\left(\frac{\pi(z-z_0)}{2iL}, e^{-\pi^2 R/L}\right)}{e^{-[(z-z_0^*)^2/4RL]}\,\vartheta_1\left(\frac{\pi(z-z_0^*)}{2iL}, e^{-\pi^2 R/L}\right)}\right]$$
$$\approx \ln\left[\frac{\sinh\left(\frac{\pi(z-z_0)}{2L}\right)}{\sinh\left(\frac{\pi(z-z_0^*)}{2L}\right)}\right] + i\frac{y_0}{L}\frac{z-x_0}{R}. \tag{43}$$

For a short cylinder, the result converges to the complex potential generated by a row of positive vortices located at positions $z_0 + 2imL$, together with a row of negative ones at positions $z_0^* + 2imL$ (with $m \in \mathbb{Z}$).

We use Eq. (8) to find the velocity of the vortex core on a short cylinder,

$$\frac{iM\dot{\boldsymbol{x}}_0}{\hbar} = \lim_{z\to z_0}\left(F'_{L\ll R}(z) - \frac{1}{z-z_0}\right)$$
$$= -\frac{\pi}{2L}\coth\left(\frac{i\pi y_0}{L}\right) + i\frac{y_0}{LR}$$
$$= \frac{i\pi}{2L}\cot\left(\frac{\pi y_0}{L}\right) + i\frac{y_0}{LR}. \tag{44}$$

For a vortex at the center of the cylinder with $y_0 = L/2$, this equation gives the familiar quantized circulating motion $\dot{\boldsymbol{x}}_0 = \hbar/2MR$, in agreement with the result from Sec. II A for $C = 1/2$. In the limit $R \to \infty$, Eq. (44) agrees with a result in Ref. [17].

C. Energy of a vortex dipole on a finite cylinder

Although Eq. (28) gives the total energy of a vortex dipole on a finite cylinder, the following more physical approach clarifies the basic physics. Consider a larger surface $-L \leqslant y \leqslant L$ which includes both the original vortex dipole and its vortex dipole image. The superfluid flow is symmetric in y, so that the energy of this extended region is twice the original energy. The complex potential on a finite cylinder (and the corresponding stream function) may be decomposed in two contributions, one coming from the vortex itself, and one from the image vortex. The notation $\mathcal{L}(z) = \ln|\vartheta_1(z/2R, q)|$ denotes the part of the stream function due to the original vortex (and not to its image), and note that $\mathcal{L}(z) \approx \ln|\eta z/2R|$ for small z, with $\eta \equiv \vartheta_1'(0,q)$. To be very specific, the stream function obtained from $F_L(z)$ is $\chi(\boldsymbol{r}, \boldsymbol{r}_j) = \mathcal{L}(z - z_j) - \mathcal{L}(z - z_j^*)$.

In complete analogy with Eq. (31), the total energy on the extended cylinder due to the original vortex dipole and its image contains the core energies of the four vortices, given by the stream function $\mathcal{L}$ evaluated at the core radius, $E_{\rm core} \equiv -\frac{1}{2}[2\pi\mathcal{L}(\xi)] \approx \pi\ln(2R/\eta\xi)$, plus the stream function $\mathcal{L}$ evaluated for the relative separation of all six possible pairs of vortices. In particular, the energy on the extended cylinder due to a vortex dipole with a positive vortex at $z_1 = x_1 + iy_1$ and a negative one at $z_2 = x_2 + iy_2$ becomes

$$E_{\rm extended} = 4E_{\rm core} - 2\pi\sum_{i<j} q_i q_j \mathcal{L}(z_{ij}) \tag{45}$$
$$= 4\pi\ln\left(\frac{2R}{\eta\xi}\right) + 2\pi[2\mathcal{L}(z_{12}) + \mathcal{L}(2iy_1) + \mathcal{L}(2iy_2) - 2\mathcal{L}(x_{12} + iy_1 + iy_2)].$$

The energy of a vortex dipole on the original finite cylinder is $E_{\rm tot} = E_{\rm extended}/2$.

VI. OUTLOOK AND CONCLUSIONS

On a plane, a superfluid vortex represents a singularity. The requirement that the condensate wave function Ψ be single valued leads to the familiar quantization of circulation around the vortex in units of $2\pi\hbar/M$. A thin superfluid film on a cylindrical surface of radius R allows for closed paths around the circumference of the cylinder as well as those around a vortex. As discussed in Sec. II A, this condition

requires that a single vortex on an infinite cylinder move in the azimuthal direction with uniform velocity $\pm\hbar/2MR$ as the simplest of many allowed quantized speeds. Here, the choice of $\pm$ sign reflects a broken symmetry, corresponding to the two equivalent "directions" (up or down) along the axis of the cylinder. Clearly, the topology of an infinite cylinder differs from that of a plane, here yielding these quantized translational motions.

For a finite cylinder of length L, the boundary conditions require pairing with an image vortex in either end of the cylinder. The resulting vortex dipole (the original positive vortex and a negative image) automatically ensures that Ψ is single valued and gives the appropriate translational velocity of the original vortex, where the choice of image (top or bottom) determines the broken symmetry and the sense of circumferential motion around the cylinder.

A superfluid film on the surface of a cylinder presents many experimental challenges. Fortunately, this geometry is topologically equivalent to a superfluid on a planar annulus, which was studied in detail in connection with three-dimensional superfluid ^{4}He [11,18]. There the interest was the sequence of equilibrium states as a function of the applied rotation.

More recently, the study of cold atoms has made dramatic progress in preparing superfluid annuli with various dimensions [19–23], leading to the creation of very thin planar annuli with closely controlled radii [24]. To date, these recent measurements largely rely on interferometric techniques to study the superfluid velocity induced by various quenches.

Earlier, rapid thermal quenches with three-dimensional condensates [25] created a single vortex line in roughly 25% of the events. Furthermore a clever technique allowed the study of the vortex dynamics in real time, at intervals of ∼90 ms. Alternatively, vortices may be created by merging multiple independent condensates [26]. We see no obvious reason why these methods cannot also apply to the study of a single vortex on a thin planar annulus. Appendix B examines the behavior of a single vortex on a planar annulus, using an inverse conformal transformation.

ACKNOWLEDGMENTS

This work originated in a discussion with V. S. Bagnato, K. Helmerson, W. D. Phillips, M. Tsubota, and A.L.F. at IIP in Natal, Brazil and continued during a visit by A.L.F. to ICFO in Barcelona. The authors thank A. Bachtold and M. Lewenstein for many insightful discussions. We also thank G. Campbell and W. D. Phillips for extensive discussions about the NIST experiments on toroidal and annular condensates. A.L.F. and P.M. performed part of this work at the Aspen Center for Physics, which is supported by the National Science Foundation through Grant No. PHY-1607611. N.G. and P.M. acknowledge support from Spanish MINECO (Severo Ochoa SEV-2015-0522, and FisicaTeAMO FIS2016-79508-P), Generalitat de Catalunya (SGR 874, and CERCA), and the Fundació Privada Cellex. N.G. is supported by a "la Caixa-Severo Ochoa" Ph.D fellowship. P.M. further acknowledges funding from "Ramón y Cajal" and "Simons Foundation" fellowships.

APPENDIX A: CONFORMAL MAPPING FROM THE PLANE TO THE CYLINDER

We review briefly the elegant treatment of Ho and Huang [12], showing that their conformal transformation leads to results that are compatible with ours. Let $Z = X + iY$ be the Cartesian coordinates on the two-dimensional plane and $z = x + iy$ the azimuthal and axial coordinates on the infinite cylinder (as in Sec. II). The phase pattern generated by a vortex located at position Z_0 in the plane is simply $\Phi_{\rm plane} = \arg(Z - Z_0)$. The phase pattern on the cylinder is now simply $\Phi_{\rm cyl} = \arg(w - w_0)$, where w is a conformal mapping from the plane to the cylinder.

Ho and Huang observe that there actually exist two (and only two) such mappings: $Z = w^{\pm} = e^{\pm iz} = e^{\pm ix}e^{\mp y}$. The map w^+ sends a tiny circle at the origin of the plane to the upper rim of the cylinder ($y \to \infty$), and a large circle on the plane to the lower rim of the cylinder ($y \to -\infty$), while w^- does just the opposite.

As such, one vortex solution in the plane actually corresponds to two vortex solutions on the cylinder, with complex potentials,

$$F_{{\rm cyl},\pm}(z) = \ln(e^{\pm iz} - e^{\pm iz_0}). \tag{A1}$$

The corresponding phase patterns are, respectively, $\Phi_{{\rm cyl},+} = \arg(e^{iz} - e^{iz_0})$, and $\Phi_{{\rm cyl},-} = \arg(e^{-iz} - e^{-iz_0})$ (note that Ref. [12] uses Θ for the phase, instead of Φ as used here). Setting $z_0 = 0$, we have

$$\Phi_{{\rm cyl},\pm} = \arg(e^{\pm iz} - 1) = {\rm Im}\{\ln[\sin(z/2)] \pm iz/2\} + {\rm const.}, \tag{A2}$$

which coincides with the result found in Eq. (9) with a nonzero background flow set by $C = \pm 1/2$, aside from an extra, irrelevant constant phase. Similarly, $\ln|Z - Z_0|$ yields the stream function on the plane, so that $\ln|w - w_0|$ gives the stream function on the cylinder.

Equations (9) and (10) in Ref. [12] give, respectively, the azimuthal and axial flow velocities v_ϕ and v_z created by a vortex on the cylinder. A straightforward calculation shows that

$$\lim_{z\to z_0} \frac{\hbar}{M}\left[F'_{{\rm cyl},\pm}(z) - \frac{1}{z - z_0}\right] = \pm i\frac{\hbar}{2MR}, \tag{A3}$$

so that the vortex core generated by the map w^+ (w^-) moves along the equator towards the right (left), with a velocity exactly equal to $\pm\hbar/(2MR)$, in agreement with our conclusion at the end of Sec. II A.

It is now simple to understand the "need" for (and amount of) quantization of the circulation around the top and bottom rims of the cylinder. Focus, for example, on the solution produced by w^+, and consider a vortex in the plane, centered away from the origin ($Z_0 \neq 0$). A small circle around the origin of the plane encloses no vortices, and therefore has zero circulation, while a large circle always encircles the vortex, and therefore has circulation 2π. As discussed above, the small and large circles are mapped by w^+ to the top and bottom parts of the cylinder, which indeed, respectively, show

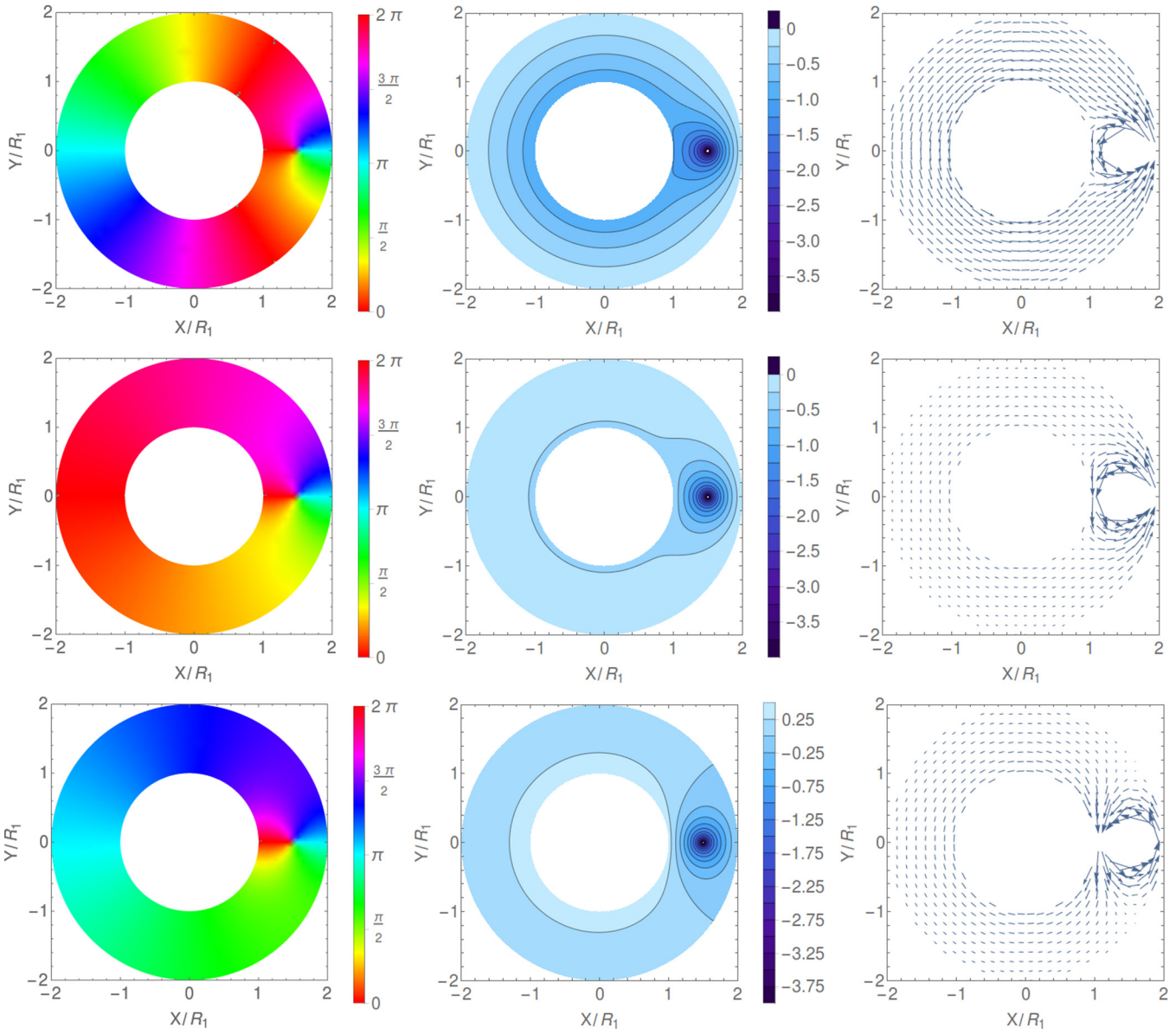

FIG. 6. Single vortex on an annulus: (top) $n_1 = 1$, (center) $n_1 = 0$, and (bottom) $n_1 = -1$. In all cases, the vortex is located at $z_0 = 1.5R_1$, and the outer radius is $R_2 = 2R_1$. From left to right, plots show the phase Φ, the stream function χ, and the velocity flow.

0 and 2π circulations. (See the phase pattern in the central row of Fig. 1.)

APPENDIX B: SINGLE VORTEX ON A PLANAR ANNULUS

The surface of a cylinder of finite length is topologically equivalent to that of a planar annulus, and therefore we expect that the vortex dynamics will be very similar in the two cases. To derive the dynamics on the annulus, the simplest way to proceed is to apply the conformal mapping discussed above.

As seen in Sec. V, the complex potential for a vortex located at z_0 on a cylinder of length L and radius R reads

$$F_L(z) = \ln\left[\frac{\vartheta_1\left(\frac{z-z_0}{2R}, e^{-L/R}\right)}{\vartheta_1\left(\frac{z-z_0^*}{2R}, e^{-L/R}\right)}\right] + n_\uparrow \frac{i\,z}{R}, \tag{B1}$$

where we have allowed for the possibility of having additional quantized flow on the upper rim of the cylinder, controlled by the integer number $n_\uparrow = C - 1/2$.

A convenient conformal mapping from the finite cylinder of radius R to the annulus of radii $R_1 = R_2 \exp(-L/R)$ and R_2 is

$$z = -i\,R \ln(Z/R_2), \tag{B2}$$

where Z is the Cartesian coordinate on the plane containing the annulus. This mapping sends the lower rim of the cylinder ($y = 0$) to R_2, the upper rim ($y = L$) to R_1, and maintains the orientation, so that anticlockwise rotation around the cylinder (increasing x) maps onto anticlockwise rotation around the annulus (increasing polar angle). Applying this mapping to Eq. (B1) immediately yields the potential for the

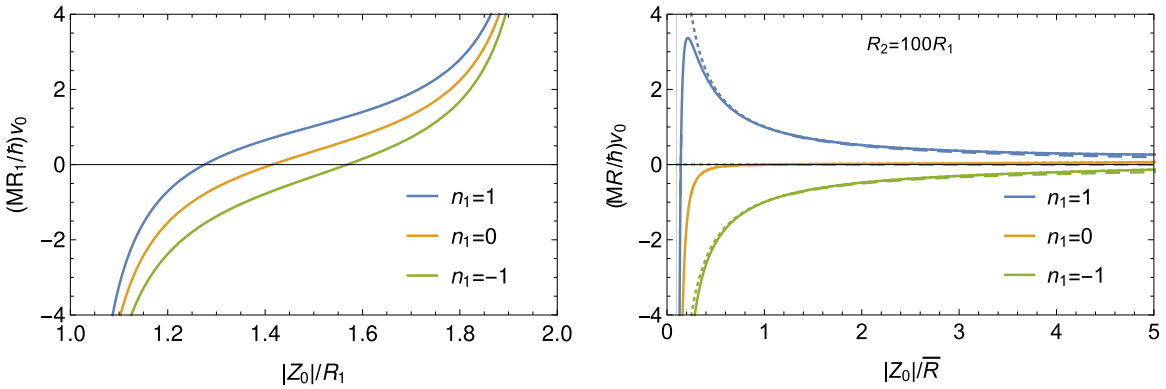

FIG. 7. Velocity of the vortex core on an annulus. (Left) Results for an outer radius $R_2 = 2R_1$, and for various values of the flow circulation around the inner radius (from top to bottom, $n_1 = 1,0,-1$). (Right) Wide annulus limit ($R_2 \gg R_1$); $\bar{R} = \sqrt{R_1 R_2}$ is the geometric mean of the radii, and the dotted and dashed lines show the limiting cases $R_1 \to 0$ and $R_2 \to \infty$, respectively, given by Eqs. (B7) and (B8).

annulus,

$$F_{\rm ann}(Z) = F_{\rm circ}(Z) + F_{\rm images}(Z) \tag{B3}$$
$$= n_1 \ln\left(\frac{Z}{R_2}\right) + \ln\left[\frac{\vartheta_1\left(-\frac{i}{2}\ln\left(\frac{Z}{Z_0}\right),\frac{R_1}{R_2}\right)}{\vartheta_1\left(-\frac{i}{2}\ln\left(\frac{ZZ_0^*}{R_2^2}\right),\frac{R_1}{R_2}\right)}\right],$$

where n_1 now determines the quantized flow circulation around the inner radius R_1 of the annulus [27]. For the given mapping, we have simply $n_1 = n_\uparrow$.

In the latter equation, the first term arises from the quantized flow around the inner boundary and the second arises from the images in both the inner and outer boundaries of the annulus, as can be shown by a direct calculation. Indeed, if we include the original vortex and all the images, the positive vortices are at $(R_1/R_2)^{2n} Z_0$ with $n \in \mathbb{Z}$. Correspondingly the negative vortices are at $(R_1/R_2)^{2n} Z_0^i$, where Z_0^i denotes either image $Z_0' = R_1^2/Z_0^*$ or $Z_0'' = R_2^2/Z_0^*$ and again $n \in \mathbb{Z}$. An analysis similar to that in Eq. (34) reproduces the previous expression $F_{\rm images}(Z)$, but now with either image, which makes clear the symmetry between the inner radius R_1 and the outer radius R_2. For the image in the inner (outer) radius, the vortex precesses in the negative (positive) direction.

The velocity potential Φ, the stream function χ and the velocity flow are shown in Fig. 6 for $n_1 = 0$ and $n_1 = \pm 1$. The plots for nonzero circulation $n_1 = \pm 1$ clearly indicate that the multiply connected geometry of the planar annulus (and of the cylinder) allows for the presence of two distinguishable and independent phase windings: the one around the vortex, and the one around the inner boundary.

A vortex on a planar annulus precesses around the center of the system, similar to the case of the cylindrical surface. A detailed calculation gives the tangential (precessional) velocity of the vortex core,

$$v_0 = \frac{\hbar}{M|Z_0|}\left[n_1 - \frac{1}{2} + \frac{i}{2}\frac{\vartheta_1'\left(-i\ln\left(\frac{|Z_0|}{R_2}\right),\frac{R_1}{R_2}\right)}{\vartheta_1\left(-i\ln\left(\frac{|Z_0|}{R_2}\right),\frac{R_1}{R_2}\right)}\right]. \tag{B4}$$

To derive this result one needs to note that, in the vicinity of the vortex core Z_0,

$$Q(Z) \equiv -\frac{i}{2Z}\frac{\vartheta_1'\left(-\frac{i}{2}\ln\left(\frac{Z}{Z_0}\right),\frac{R_1}{R_2}\right)}{\vartheta_1\left(-\frac{i}{2}\ln\left(\frac{Z}{Z_0}\right),\frac{R_1}{R_2}\right)} \approx \frac{1}{Z-Z_0} - \frac{1}{2Z_0}, \tag{B5}$$

as may be seen expanding the logarithms inside the ϑ functions to *second order* in $Z - Z_0$, so that $\lim_{Z\to Z_0}(Q(Z) - \frac{1}{Z-Z_0}) = -\frac{1}{2Z_0}$.

When $|Z_0| = \bar{R} \equiv \sqrt{R_1 R_2}$ (the geometric mean of the inner and outer radii), the identity $\vartheta_1'(-i\ln\sqrt{q},q) = -i\vartheta_1(-i\ln\sqrt{q},q)$ valid for any real q $(0 < q < 1)$ immediately yields the simple result for the precessional velocity,

$$v_0 = n_1(\hbar/M\sqrt{R_1 R_2}). \tag{B6}$$

It is intriguing to note that the mapping transforms the circle of radius $\bar{R}$ onto the circle $y = L/2$ going round a finite cylinder at half its length. As such, the latter result is the direct analog of Eq. (39). Note, however, there is an important difference: When $n_1 = n_\uparrow = 0$ a vortex along this line is stationary on the annulus, but it moves on the cylinder.

The series expansion of ϑ_1 for small q may now be used: $\vartheta_1(\alpha,q) = 2q^{1/4}(\sin\alpha - q^2\sin 3\alpha) + \mathcal{O}(q^{25/4})$. Retaining only the lowest order, we find the limiting behavior for $R_1 \to 0$,

$$v_0 = \frac{\hbar}{M|Z_0|}\left(n_1 + \frac{|Z_0|^2}{R_2^2 - |Z_0|^2}\right). \tag{B7}$$

When $n_1 = 0$, one recovers the well-known result for a vortex in a trapped disk-shaped BEC.

To take the limit $R_2 \to \infty$ while retaining a dependence on $|Z_0|$, one needs instead to expand both ϑ_1 functions to order $q^{9/4}$. Doing so gives a rather complicated expression. In the limit $R_2 \to \infty$ we find

$$v_0 = \frac{\hbar}{M|Z_0|}\left(n_1 - \frac{R_1^2}{|Z_0|^2 - R_1^2}\right), \tag{B8}$$

which is the usual result for a vortex outside a cylinder of radius R_1. Finally in the limit $R_1 \ll |Z_0| \ll R_2$, one finds $v_0 = n_1\hbar/M|Z_0|$.

Figure 7 shows the various results found above for the precession velocity of a vortex on an annulus. A confirmation of the validity of the above findings may be obtained by showing that the complex potential for the annulus with $n_1 = 0$ reduces to the one for the disk when $R_1 \to 0$. Indeed, using the lowest order of the series expansion of the theta function, simple algebra shows that

$$F_{\rm ann}(Z) \approx \ln\left[\frac{\sin\left[-\frac{i}{2}\ln\left(\frac{Z}{Z_0}\right)\right]}{\sin\left[-\frac{i}{2}\ln\left(\frac{ZZ_0^*}{R_2^2}\right)\right]}\right] = \ln\left[\frac{Z-Z_0}{Z-\frac{R_2^2}{Z_0^*}}\right] + \text{ a const.} \tag{B9}$$

Since the complex potential for the annulus reduces to the one of the disk (apart from an irrelevant constant), the velocity must do the same.

[1] H. Lamb, *Hydrodynamics*, 6th. ed. (Dover Publications, New York, 1945).

[2] R. J. Donnelly, *Quantized Vortices in Helium II* (Cambridge University Press, Cambridge, 1991).

[3] L. Pitaevskii and S. Stringari, *Bose-Einstein Condensation* (Clarendon Press, Oxford, 2003).

[4] C. J. Pethick and H. Smith, *Bose-Einstein Condensation in Dilute Gases*, 2nd ed. (Cambridge University Press, Cambridge, 2008).

[5] A. L. Fetter, Rotating trapped Bose-Einstein condensates, Rev. Mod. Phys. **81**, 647 (2009).

[6] G. Baym and C. J. Pethick, Ground-State Properties of Magnetically Trapped Bose-Condensed Rubidium Gas, Phys. Rev. Lett. **76**, 6 (1996).

[7] L. Calderaro, A. L. Fetter, P. Massignan, and P. Wittek, Vortex dynamics in coherently coupled Bose-Einstein condensates, Phys. Rev. A **95**, 023605 (2017).

[8] T. C. Lubensky and J. Prost, Orientational order and vesicle shape, J. Phys. II (France) **2**, 371 (1992).

[9] A. M. Turner, V. Vitelli, and D. R. Nelson, Vortices on curved surfaces, Rev. Mod. Phys. **82**, 1301 (2010).

[10] E. T. Whittaker and G. N. Watson, *A Course of Modern Analysis*, 4th ed. (Cambridge University Press, Cambridge, 1962).

[11] A. L. Fetter, Low-lying superfluid states in a rotating annulus, Phys. Rev. **153**, 285 (1967).

[12] T.-L. Ho and B. Huang, Spinor Condensates on a Cylindrical Surface in Synthetic Gauge Fields, Phys. Rev. Lett. **115**, 155304 (2015).

[13] P. G. de Gennes, *Superconductivity of Metals and Alloys* (W. A. Benjamin, Inc., New York, 1966).

[14] J. Machta and R. A. Guyer, Superfluid films on a cylindrical surface, J. Low Temp. Phys. **74**, 231 (1989).

[15] M. Łacki, H. Pichler, A. Sterdyniak, A. Lyras, V. E. Lembessis, O. Al-Dossary, J. C. Budich, and P. Zoller, Quantum Hall physics with cold atoms in cylindrical optical lattices, Phys. Rev. A **93**, 013604 (2016).

[16] R. B. Laughlin, Quantized Hall conductivity in two dimensions, Phys. Rev. B **23**, 5632 (1981).

[17] L. A. Toikka and J. Brand, Asymptotically solvable model for a solitonic vortex in a compressible superfluid, New J. Phys. **19**, 023029 (2017).

[18] P. J. Bendt, Superfluid helium critical velocity in a rotating annulus, Phys. Rev. **127**, 1441 (1962).

[19] C. Ryu, M. F. Andersen, P. Cladé, V. Natarajan, K. Helmerson, and W. D. Phillips, Observation of Persistent Flow of a Bose-Einstein Condensate in a Toroidal Trap, Phys. Rev. Lett. **99**, 260401 (2007).

[20] S. Moulder, S. Beattie, R. P. Smith, N. Tammuz, and Z. Hadzibabic, Quantized supercurrent decay in an annular Bose-Einstein condensate, Phys. Rev. A **86**, 013629 (2012).

[21] S. Eckel, F. Jendrzejewski, A. Kumar, C. J. Lobb, and G. K. Campbell, Interferometric Measurement of the Current-Phase Relationship of a Superfluid Weak Link, Physical Review X **4**, 031052 (2014).

[22] L. Corman, L. Chomaz, T. Bienaimé, R. Desbuquois, C. Weitenberg, S. Nascimbène, J. Dalibard, and J. Beugnon, Quench-Induced Supercurrents in an Annular Bose Gas, Phys. Rev. Lett. **113**, 135302 (2014).

[23] J. L. Ville, T. Bienaimé, R. Saint-Jalm, L. Corman, M. Aidelsburger, L. Chomaz, K. Kleinlein, D. Perconte, S. Nascimbène, J. Dalibard, and J. Beugnon, Loading and compression of a single two-dimensional Bose gas in an optical accordion, Phys. Rev. A **95**, 013632 (2017).

[24] M. Aidelsburger, J. L. Ville, R. Saint-Jalm, S. Nascimbène, J. Dalibard, and J. Beugnon, Relaxation Dynamics in the Merging of N Independent Condensates, Phys. Rev. Lett. **119**, 190403 (2017).

[25] D. V. Freilich, D. M. Bianchi, A. M. Kaufman, T. K. Langin, and D. S. Hall, Real-time dynamics of single vortex lines and vortex dipoles, Science **329**, 1182 (2010).

[26] D. R. Scherer, C. N. Weiler, T. W. Neely, and B. P. Anderson, Vortex Formation by Merging of Multiple Trapped Bose-Einstein Condensates, Phys. Rev. Lett. **98**, 110402 (2007).

[27] Using the Jacobi imaginary transformation, the complex potential for the annulus may be written as

$$F_{\rm ann}(Z) = n_1 \ln\left(\frac{Z}{R_2}\right) + \frac{\ln\left(\sqrt{\frac{Z_0^*}{Z_0}}\frac{Z}{R_2}\right)\ln\left(\frac{R_2}{|Z_0|}\right)}{\ln\left(\frac{R_2}{R_1}\right)} + \ln\left[\frac{\vartheta_1\left(\gamma\ln\left(\frac{Z}{Z_0}\right),q\right)}{\vartheta_1\left(\gamma\ln\left(\frac{ZZ_0^*}{R_2^2}\right),q\right)}\right],$$

where $\gamma = \pi/[2\ln(R_2/R_1)]$ and $q = e^{-2\pi\gamma}$. This formula differs from the one provided in Ref. [11] by the phase factor $\sqrt{Z_0^*/Z_0}$, which represents a rotation of the branch cut of the logarithm. Whenever Z_0 lies on the real positive axis, however, the phase factor is unity and the two formulas coincide. Note that the roles of χ and Φ are interchanged with respect to Ref. [11], so that we have removed an i from Eq. (10) of that work.